



Nanoscale

**Sustainable Power Generation via Hydro-Electrochemical Effects**

Journal:	<i>Nanoscale</i>
Manuscript ID	NR-ART-11-2021-007748.R2
Article Type:	Paper
Date Submitted by the Author:	05-Feb-2022
Complete List of Authors:	Sohn, Ahrum ; Texas A&M University, Mechanical/Materials Science and Engineering Zhang , Yufan ; Texas A&M University, Mechanical/Materials Science and Engineering Chakraborty, Anirban ; Texas A&M University, Mechanical/Materials Science and Engineering Yu, Choongho; Texas A&M University, Mechanical/Materials Science and Engineering

SCHOLARONE™  
Manuscripts

## PAPER

## Sustainable Power Generation via Hydro-Electrochemical Effects

Ahrum Sohn<sup>a</sup>, Yufan Zhang<sup>b</sup>, Anirban Chakraborty<sup>a</sup>, Choongho Yu<sup>a,b,\*</sup>

Received 00th January 20xx,  
Accepted 00th January 20xx

DOI: 10.1039/x0xx00000x

Recent efforts for energy scavenging with eco-friendly and abundant water look very promising for powering wearables and distributed electronics. However, the time duration of the electricity generation is typically too short, and the current level is not sufficient to meet the required threshold for proper operation of electronics despite the relatively large voltage. This work newly introduced an electrochemical method in combination with the hydro-effect in order to elongate the energy scavenging time and boost the current. Our device consists of corroded porous steel electrodes whose corrosion overpotential was lowered when the water concentration was raised and vice versa. Then a potential difference was created between two electrodes, generating electricity via the hydro-electrochemical method up to an open-circuit voltage of 750 mV and a short-circuit current of 90  $\mu\text{A}/\text{cm}^2$ . Furthermore, electricity was continuously generated for more than 1500 minutes by slow water diffusion against gravity from the bottom electrode. Lastly, we demonstrated that our hydro-electrochemical power generators successfully operated electronics, showing the feasibility of offering electrical power for sufficiently long time periods in practice.

### Introduction

Internet of things (IoT) and wearable devices have necessitated sustainable delivery of electrical power from the environment and/or wasted energy such as energy scavenging from solar energy, thermal energy, electrochemical energy, and mechanical energy<sup>1-4</sup>. Among them, water is an attractive energy source because it is abundant, low-cost, and environmentally benign without requiring particular weather, temperature, or vibration conditions for electrical energy generation<sup>5-10</sup>. The water-enabled energy conversion is a recently emerged field of study where ion transport in an ion conductor (serving as an electrolyte) generates voltage between electrodes. The ion transport is governed by the diffusion of water molecules, which can be triggered by temperature difference<sup>11-15</sup> or concentration difference of water<sup>7, 8, 10, 16-19</sup>. Various methods generating electricity from water including triboelectrification<sup>20-23</sup>, the streaming current<sup>24, 25</sup>, ion-gradient induced electric power generation<sup>19, 26</sup> and the development of the interfacial structure<sup>27, 28</sup> have been reported. When water diffusion is utilized, the generated voltage ( $\sim 1$  V) is adequate to operate small wearable electronic devices, compared to the tiny voltage from thermoelectrics<sup>12, 29</sup> and large voltage from triboelectrics<sup>1, 30, 31</sup>. Nevertheless, the duration of the water-enabled current generation is rather short (on the order of minutes), which makes the actual electrical energy insufficiently low to operate electronics for desired time periods. For example, the electric power generation using water droplet based on triboelectric effects can generate the peak voltage

of several volt and the peak current of several tens of  $\mu\text{A}/\text{cm}^2$  with a single droplet (30  $\mu\text{L}$ ), but the generated energy is only nano joule due to the extremely short energy generation time (milliseconds)<sup>20, 32, 33</sup>. Xu et al. reported moisture-induced directional movement of protons upon exposure to different humidity environments, generating open-circuit voltage on the order of 0.8 V and short-circuit current on the order of 150  $\mu\text{A}/\text{cm}^2$ , which are acceptable to operate electronics in practice<sup>17</sup>. However, the short discharging time (100 seconds) compared to the relatively long charging time (30 minutes) remains a challenge in addition to the unusually large change (70 %) of relative humidity. Recently, Zhang *et al.* introduced a new concept of thermo-hydro-electrochemical energy scavenging by differentiating the electrochemical potential of two electrodes due to the thermally-induced water migration<sup>34</sup>.

Here we employed hydro-electrochemical effect on corroded carbon steel electrodes. When the water concentration in one electrode is different from the other electrode, voltage and current were continuously obtained until the electrochemical potential difference between the two electrodes became identical. When water was in contact with the corroded steel electrodes, the corrosion overpotential decreased, resulting in the potential difference between the two electrodes. To maintain the potential difference for a longer period of time, the water diffusion was interrupted by embedding aligned chemically expanded graphite (CEG) perpendicular to the water transport direction in the interlayer. Upon supplying water to one of the electrodes, the maximum open-circuit voltage and short-circuit current of 0.8 V and 90  $\mu\text{A}/\text{cm}^2$  were observed, and then they were gradually decreased over 1000 minutes. Finally, we demonstrated our power generator could operate an electrochromic cell and a hygrometer.

<sup>a</sup> Department of Mechanical Engineering, Texas A&M University, College Station, Texas 77843, USA

<sup>b</sup> Department of Materials Science and Engineering, Texas A&M University, College Station, Texas 77843, USA

\*Corresponding author, E-mail address: [chyu@tamu.edu](mailto:chyu@tamu.edu) See

DOI: 10.1039/x0xx00000x

## Experimental

Our hydro-electrochemical cell is composed of two electrodes and one interlayer. For the electrode, carbon steel wool with a thickness of 300  $\mu\text{m}$  (wire diameter:  $\sim 40$   $\mu\text{m}$ ) was sandwiched between two carbon steel meshes (wire diameter: 230  $\mu\text{m}$ ; square hole dimension: 400  $\mu\text{m}$   $\times$  400  $\mu\text{m}$ ) by applying a pressure of 150 MPa. The dimension of the mesh is 2.5 cm  $\times$  1.5 cm with an active area of 1.5 cm  $\times$  1.5 cm by misaligning 1 cm from each side for electrical connection. Subsequently, 1M HCl (500  $\mu\text{l}$ ) was dropped onto the electrodes to corrode the carbon steel, and dried in a fume hood. The interlayer was fabricated by mixing an aqueous polystyrene sulfonic acid (PSS-H) solution (30% aqueous solution, Alfa Aesar) and chemically expanded graphite (CEG) using a pen-type sonicator (XL2000, Misonix Micron) with 100 W for 30 minutes. To synthesize the CEG, 10-g graphite flake (100 mesh, > 99.9% purity) and 85 g of  $\text{CrO}_3$  (> 99% purity, Alfa Aesar) were added into 70-mL hydrochloric acid (37 wt %). Then the mixture was stirred at room temperature for 2 hours (magnetic stirrer bar). The solution was filtered with a vacuum filtration setup, and the collected flake was washed with deionized water (washed multiple times using vacuum filtration) to obtain graphite intercalated with  $\text{H}_2\text{Cr}_2\text{O}_7$ <sup>35</sup>. The intercalated flakes were immersed in an aqueous  $\text{H}_2\text{O}_2$  (30% concentration) with a graphite concentration of 0.2 grams per 40 mL pure  $\text{H}_2\text{O}_2$  for

expansion by releasing gas ( $\text{O}_2$  gas)<sup>36</sup>. The expanded particles were collected and dried at room temperature overnight to obtain CEG particles. The amount of CEG in 30-wt% PSS-H was fixed to 10 wt%. The CEG/PSS-H mixture solution (7.5 mL) was dropped into a container whose dimension is 20 mm  $\times$  20 mm  $\times$  2 mm. In an ambient condition, the CEG/PSS-H solution was dried for 24 hours with a water uptake of  $\sim 30$  wt%. The corroded electrodes and the CEG/PSS-H interlayer were assembled by applying a pressure of 500 Pa. The gel-like CEG/PSS-H smeared into the porous electrodes, playing a role in holding them together. The thickness of the device was about 2 mm.

To operate the hydro-electrochemical energy generator, water (200  $\mu\text{L}$ ) was applied onto the top electrode dropwise with a rate of 100  $\mu\text{L}/\text{second}$ . Alternatively, water was soaked from the bottom electrode of the generator, which allowed for generating electricity for a longer period of time by continuous water supply due to capillary action through hydrophilic cellulose from a water reservoir. The water was delivered to the generator at a rate of  $\sim 0.5$  mL/hour. Voltage and current from the hydro-electrochemical generator were measured by connecting two digital multimeters (Keithley 2000) and a load resistor box (resistance range: 1 $\Omega$  to 10 M $\Omega$ ).

## Results and discussion

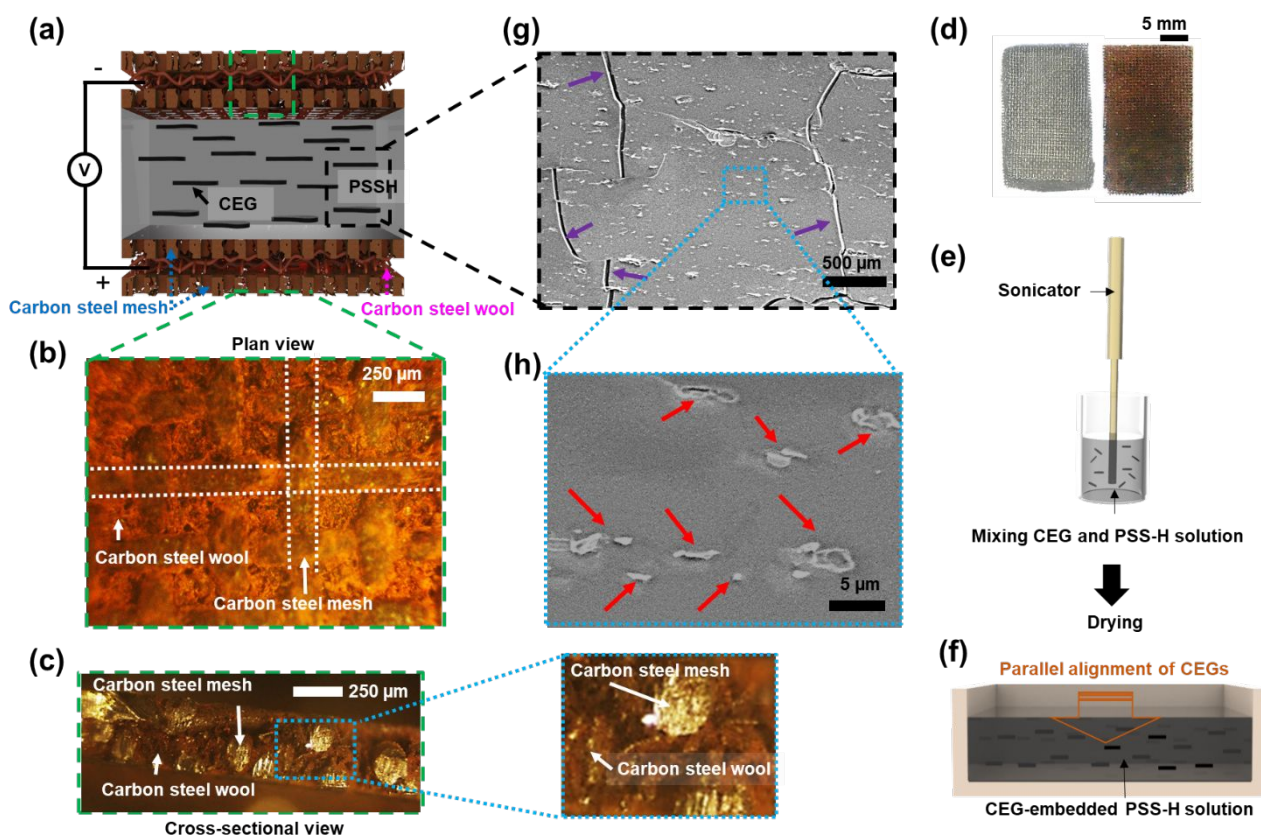
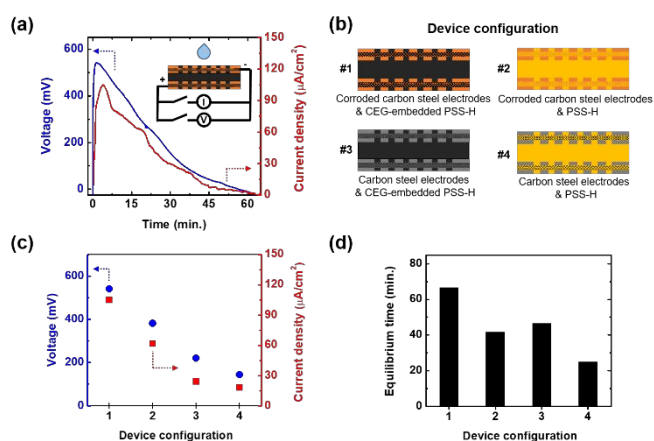


Figure 1. (a) An illustration of our hydro-electrochemical device consisting of an interlayer made of CEGs-embedded PSS-H and two identical corroded steel electrodes where positive and negative terminals were connected for electrical measurements. Optical microscope image showing (b) an outer surface of the electrode showing interwoven mesh wires and wool in between, and (c) a cross-section of the electrode showing steel wool sandwiched by steel meshes. The white dashed lines indicate the boundary of two mesh wires. (d) Photographs of the carbon steel mesh before (left side) and after (right side) corrosion. The interlayer was prepared by (e) dispersing CEG in the PSS-H solution using a sonicator and then (f) drying the mixture solution in a container without any disturbance so that CEG can be self-aligned in a direction parallel to the bottom of the container. (g) A cross-sectional SEM image of the interlayer where the cracks indicated by the purple arrows suggest water transporting along the vertical direction. (h) A magnified image of 'g' showing aligned CEG embedded in PSS-H.

## PAPER

Our hydro-electrochemical cell consists of two identical carbon steel electrodes and an interlayer made of polystyrene sulfonic acid (PSS-H) and CEG, as illustrated in Figure 1a. The electrode was fabricated by sandwiching carbon steel wool between two carbon steel meshes. The sandwiched structure with fine wires from the wool was intended to increase the surface contact area with water. To improve the electrical connection between the meshes and the wool, the sandwiched structure was compressed, as shown in the plan view (Figure 1b) and cross-sectional view (Figure 1c) under an optical microscope. In the cross-sectional image, fine wires from the wool are shown between mesh wires whose diameter is bigger. On the outer plane of the electrode, woven mesh wires in a checker pattern are seen, and steel wool was well entangled with the mesh, ensuring many electrical contacts between them. To facilitate the hydro-electrochemical energy generation from the carbon steel, the electrodes were corroded with a hydrochloric acid solution prior to integrating them with the interlayer, which was confirmed by the color change from silvery to reddish color (Figure 1d). The interlayer was prepared by drop-casting an aqueous mixture solution containing PSS-H and CEG in a container (Figure 1e). During the water evaporation process without disturbance, CEG particles were aligned in the direction parallel to the electrode due to the gravity, as illustrated in Figure 1f and shown in the scanning electron microscope (SEM) image (Figure 1g,h). The cracks in the PSS-H indicated by the arrows in Figure 1g suggest the presence of water passages

The device with the two corroded steel electrodes and CEG-embedded PSSH film was tested as a function of time, as shown in the open-circuit voltage (blue, left) and the short-circuit current (red, right) in Figure 2a when 200  $\mu\text{l}$  water was dropped on the top side ( $1.5 \times 1.5 \text{ cm}^2$ ) of the electrode (see the inset of Figure 2a). On the corroded electrode,  $\beta\text{-FeOOH}/\text{Fe}^{2+}$  redox couple was present<sup>34</sup> and electrons were drawn and donated between the two corroded electrode, showing the short-circuit current upon creating the potential difference. When the water reached the interlayer made of non-porous and hygroscopic PSS-H, the water transport was driven by slow diffusion due to the concentration difference and gravity. Our device is advantageous in operation as it works with a drop of water without necessitating special external stimuli or energy input. For instance, ion-gradient based electric power generation<sup>19,26</sup> requires spontaneous and continuous changes in relative humidity (over 70 %) to generate a sufficient voltage. The maximum open-circuit voltage ( $\sim 540 \text{ mV}$ ) and the maximum short-circuit current ( $\sim 105 \mu\text{A}/\text{cm}^2$ ) were observed at 4 minutes, and both voltage and current were gradually decreased over 65 minutes. The reductions can be attributed to the water diffusion from the top to the bottom due to the gravity and concentration difference. Eventually, the electrochemical potentials of both electrodes became identical, resulting in zero voltage and current when the water was distributed uniformly. To identify the role of each component in the device, we constructed four different configurations, as shown in Figure 2b, by changing one component for each configuration. The #1 configuration is our main device with the CEG-embedded PSS-H interlayer and two identical corroded carbon steel electrodes. The #2 configuration replaced the interlayer with pure PSS-H. The #3 configuration employed non-corroded steel electrodes, and #4 used the pure PSS-H interlayer with non-corroded steel electrodes. Figure S1 shows the voltage and current from the four different devices as a function of time, and Figure 2c presents the maximum open-circuit voltage (blue, left), and the maximum short-circuit current (red, right) for the four configurations. In addition, we measured “equilibrium time” (Figure 2d), which is the time period for the voltage to return to its initial value as the voltage became zero (initial value) when an equilibrium in the water diffusion was reached in the interlayer. This equilibrium time is closely related to the duration of device operation after an initial event such as applying a water droplet. The #1 configuration displayed the highest voltage, current, and equilibrium time. The corroded electrodes (#1, #2) provided larger voltage and current compared with those of non-



perpendicular to the CEG plane<sup>11</sup>. This implies that water transport was effectively retarded by the aligned CEG. When water droplet was applied to the top electrode, the difference between the water uptakes of the top and bottom electrodes was maintained for a longer period of time, which has extended the electricity generation, as explained in more details below.

Figure 2. (a) Open-circuit voltage (blue, left) and short-circuit current (red, right) of the hydro-electrochemical device as a function of time when water droplets were applied to the top electrode, as illustrated in the inset. (b) Four different electrode configurations (labeled as #1, #2, #3, and #4) of the device with corroded and pristine steel electrodes and PSS-H interlayers with and without CEG. (c) Maximum open-circuit voltage (blue, left) and short-circuit current (red, right) from the four different configurations shown in 'b'. (d) Elapsed time (called equilibrium time) until the voltage reached zero for the four different devices in 'b'.

corroded electrodes (#3, #4) which was contributed by the water movement and proton transport<sup>11, 34</sup>. In the same experiment with the PSS-H as an interlayer and graphite as electrodes, voltage generation was only around 10 mV, as shown in Figure S2. This result is consistent with the outcomes in a paper revealing that the electrochemical effect generated larger voltages in an ion conductor with corroded electrodes<sup>34</sup>. The CEG (#1, #3) extended the equilibrium time, extending the device operation time, indicating the water diffusion was retarded. It is clear that the #1 configuration consisting of corroded steel electrodes and the CEG interlayer delivered the best performances.

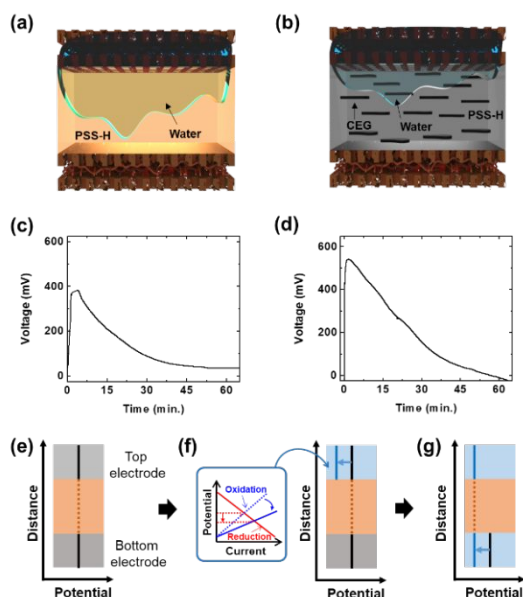


Figure 3. Water diffusion from the top electrode to the bottom when (a) PSS-H and (b) CEG/PSS-H composite were used, illustrating CEG impeded the water diffusion due to the aligned CEG perpendicular to the water diffusion path. Open-circuit voltage from the devices (c) without and (d) with CEG in the interlayer as a function of time after water droplets were applied to the top electrode. The electrochemical potential of the top and bottom electrodes (e) before and (f) after water was dropped on the top electrode. The water in the top electrode reduced the corrosion overpotential, creating the potential difference between the top and bottom electrodes, as illustrated in the Evans diagram with the newly established oxidation line (blue-solid line). (g) When the water diffused to the bottom electrode, the potential difference approached zero.

We also noticed that CEG-embedded PSS-H resulted in higher output voltage than pure PSS-H. Figure 3a and b illustrate the difference in the water diffusion with and without CEG in the PSS-H layer. When water was applied to the top side of the device, the water diffused in the PSS-H layer toward the bottom due to gravity (Figure 3a). On the other hand, water transport in CEG-embedded PSS-H was effectively impeded by the CEG, so it takes longer for water to reach the bottom electrode (Figure 3b). The pure PSS-H device generated a maximum open-circuit voltage of ~400 mV with an equilibrium time of 45 minutes (Figure 3c), whereas CEG raised the maximum open-circuit voltage to 540 mV and elongated equilibrium time over 60 minutes (Figure 3d). Initially, before applying water to the top electrode, the electrochemical potentials of the two electrodes are identical (Figure 3e). When water soaked into the top

electrode, the electrode potential was lowered as a result of a smaller overpotential, as depicted in the Evans diagram<sup>34</sup>. The newly established oxidation line (solid blue line in Figure 3f) created a potential difference (i.e., non-zero output voltage) between the top and bottom electrodes. At this stage, voltage rapidly rose during the time period from 0 to approximately 5 minutes in Figure 3c,d because the electrode is very porous. As the water diffused all the way through the interlayer to the bottom electrode, the electrode potentials of the two electrodes were closer, showing gradually decaying voltage. Therefore, the time duration of voltage generation strongly depends on the time period for water to reach the bottom electrode.

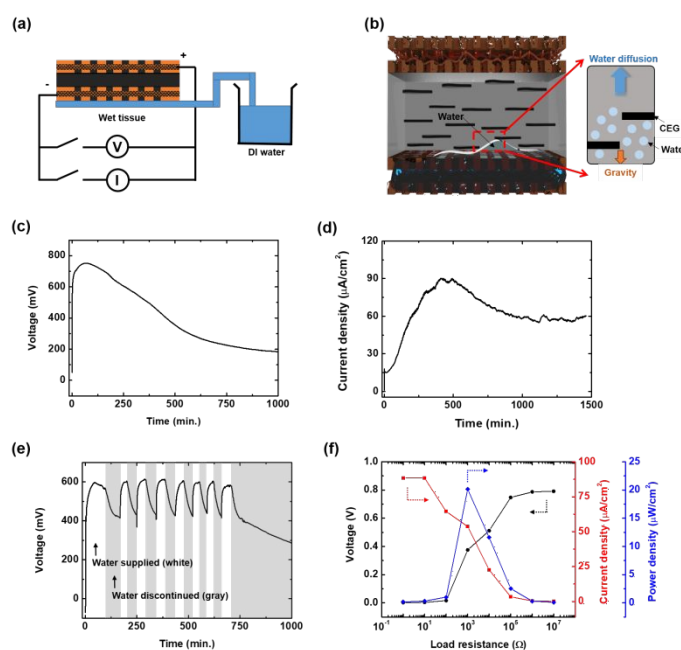


Figure 4. (a) Water was continuously supplied from the bottom electrode through a wet tissue from a reservoir. (b) When water diffused from the bottom to the top, downward gravity and CEG impeded the diffusion speed. (c) Open-circuit voltage and (d) short-circuit current from the device with a continuous supply of water, and (e) open-circuit voltage when the water supply was intermittently discontinued. (f) Voltage (black), current (red), and power (blue) from the device as a function of load resistance.

To have a more prolonged operation of the device, it is evident that dissimilar electrochemical potentials between the two electrodes should be maintained for a longer time period. Here we reversed the water diffusion direction from the bottom to the top by continuously supplying water from the bottom through a wet wipe (Kimwipes, Kimtech) from a water reservoir, as depicted in Figure 4a. While water diffused from the bottom to the top by the concentration difference in the interlayer, gravity pulled the water downward (Figure 4b), and thereby water transport became sluggish, elongating the time period for the water to diffuse all the way to the top electrode. According to the open-circuit voltage as a function of time (Figure 4c), the maximum voltage went up till ~750 mV, which is higher than the previous case where water transport and gravity directions are coincident. The voltage rise was observed till 60 minutes, compared to only ~4 minutes from the device in Figure 3.

Furthermore, the non-zero voltage was maintained much longer, over 1000 minutes. The maximum short-circuit current was similar regardless of the water diffusion direction, but the non-zero current was observed for a much longer period of time, and maintained to be  $\sim 60 \mu\text{A}/\text{cm}^2$  even after 1500 minutes of operation (Figure 4d). Such a long operation time is advantageous compared to other water based energy harvesters. For example, triboelectric devices utilizing water droplets can generate several  $\mu\text{A}$  for short periods of time on the order of milliseconds in a form of alternating current that requires additional electronic components such as rectifiers and capacitors. Moreover, it is necessary to change the position of water droplets continuously to generate electricity<sup>20-22</sup>. On the other hand, the devices utilizing streaming current can generate voltage for several hours to a day, but the generated current is very small in the range between a few hundred nA and a few  $\mu\text{A}$ , which make it difficult to continuously generate desirable power of  $\mu\text{W}$  for operating electronics in practice<sup>24, 25</sup>.

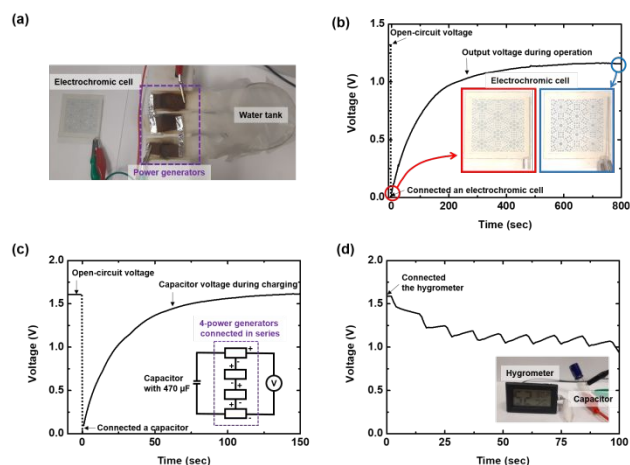


Figure 5. (a) A photograph showing an electrochromic display powered by three serially connected hydro-electrochemical power generators. (b) Output voltage from the power generator in 'a', showing two different patterns in the electrochromic display right after the display was connected (red circle) and after 800 seconds (blue circle). (c) The voltage of a  $470\text{-}\mu\text{F}$  capacitor charged by four serially-connected hydro-electrochemical power generators. (d) The discharge voltage of the capacitor during the operation of the hygrometer.

To verify the role of the water, we supplied water to the bottom electrode and then discontinued to supply water repeatedly. Upon disconnecting the water supply (gray areas in Figure 4e), the voltage dropped, and then it was recovered when water was resupplied. When water was not supplied, water diffused into the interlayer towards the top electrode, lessening the water concentration difference between the top and bottom electrodes and making the corrosion potentials of the two electrodes closer (i.e., lower output voltage). We also measured voltage and current as a function of external load resistance ( $1 \Omega \sim 10^7 \Omega$ ) in order to characterize device performances when it is under operation in practice. Figure 4f displays the maximum voltage and areal current and corresponding areal power output. With increasing resistance, the output voltage (black symbol) was enlarged gradually, whereas the output current (red symbol) was diminished. The output power (blue symbol)

was obtained by multiplying the voltage and current, yielding a maximum power of  $20 \mu\text{W}/\text{cm}^2$  with a load resistance of  $10^3 \Omega$ . Finally, we have demonstrated that it is feasible to operate electronic devices such as an electrochromic display and a hygrometer. The electrochromic display changes color when charges are supplied because the redox states of the electrodes are altered. Figure 5a shows the experimental setup for powering the display. Three power generators were connected in series to boost up the voltage, and water was supplied through wet wipes to the bottom electrodes of the generators. The voltage response as a function of time during the operation is shown in Figure 5b. When the electrochromic cell was connected to the power generator (red circle), the corresponding electrochromic display is displayed in the left inset of Figure 5b. When the voltage reached 1.15 V after 800s (blue circle), the pixel color of the display was altered, showing a different pattern (right inset of Figure 5b). We also stored the harvested energy in a capacitor with four power generators connected in series. Figure S3 shows the configuration of the setup with the hygrometer and four power generators. The recommended and minimum operation voltages for the hygrometer are 3 V and 1 V, respectively. Figure 5c shows the voltage of the capacitor, whose capacitance is  $470 \mu\text{F}$  when four power generators were connected, and the inset depicts the corresponding electrical circuit diagram. After 150 seconds, the capacitor was charged to 1.5 V. When a hygrometer was connected to the charged capacitor, the hygrometer worked for 100 seconds as the output voltage of the capacitor decayed to the minimum voltage of 1 V (Figure 5d).

## Conclusions

This work offers a promising approach to extend the power generation time and boost current by incorporating the corrosion potential difference caused by water diffusion. To facilitate the change in the corrosion potential by water, the carbon steel electrodes were corroded and steel wool made of fine wires were used. The interlayer was made of hydroscopic PSS-H where aligned CEG was embedded to impede the speed of water diffusion to maintain the potential difference between the top and bottom electrodes for a longer period of time. To identify the roles of corroded steel and CEG, four different device configurations were tested, substantiating the corroded steel and CEG gave rise to larger voltage and current as well as longer operation time. When water was continuously supplied from the bottom again the gravity, the water diffusion speed was lowered, resulting in a large open-circuit voltage of 750 mV and short-circuit current density of  $90 \mu\text{A}/\text{cm}^2$  for over 1500 minutes, and a maximum power of  $20 \mu\text{W}/\text{cm}^2$  with a load resistance of  $10^3 \Omega$  from a single device whose dimension is 1.5 cm by 1.5 cm. When four hydro-electrochemical power generators were connected in series, the output voltage was  $\sim 1.5\text{V}$ , which is sufficiently large to operate electronics such as electrochromic display and hygrometer over 800 seconds. Our finding suggests not only a new approach via hydro-

electrochemical effects to obtaining outstanding performances with low-cost carbon steel but also provides opportunities to utilize various metal electrodes for further improving power generation.

## Author Contributions

A.S. conceived the idea, carried out the experiments and analyses, and wrote the paper. Y.Z assisted the experiments. A.C synthesized the chemically expanded graphite. C.Y conceived the idea, supervised all experiments and analyses, and reviewed and edited the manuscript.

## Conflicts of interest

There are no conflicts to declare.

## Acknowledgements

The authors acknowledge financial support from US National Science Foundation (CBET 1805963).

## References

1. R. Hinchet, H. J. Yoon, H. Ryu, M. K. Kim, E. K. Choi, D. S. Kim and S. W. Kim, *Science*, 2019, **365**, 491+.
2. M. Jeong, I. W. Choi, E. M. Go, Y. Cho, M. Kim, B. Lee, S. Jeong, Y. Jo, H. W. Choi, J. Lee, J. H. Bae, S. K. Kwak, D. S. Kim and C. Yang, *Science*, 2020, **369**, 1615+.
3. B. Y. Yu, J. J. Duan, H. J. Cong, W. K. Xie, R. Liu, X. Y. Zhuang, H. Wang, B. Qi, M. Xu, Z. L. Wang and J. Zhou, *Science*, 2020, **370**, 342+.
4. Z. H. Zhang, X. M. Li, J. Yin, Y. Xu, W. W. Fei, M. M. Xue, Q. Wang, J. X. Zhou and W. L. Guo, *Nat Nanotechnol*, 2018, **13**, 1109-1119.
5. S. S. He, Y. Y. Zhang, L. B. Qiu, L. S. Zhang, Y. Xie, J. Pan, P. N. Chen, B. J. Wang, X. J. Xu, Y. J. Hu, C. T. Dinh, P. De Luna, M. N. Banis, Z. Q. Wang, T. K. Sham, X. G. Gong, B. Zhang, H. S. Peng and E. H. Sargent, *Adv Mater*, 2018, **30**.
6. Y. X. Huang, H. H. Cheng and L. T. Qu, *Acs Mater Lett*, 2021, **3**, 193-209.
7. Y. Liang, F. Zhao, Z. H. Cheng, Y. X. Deng, Y. K. Xiao, H. H. Cheng, P. P. Zhang, Y. X. Huang, H. B. Shao and L. T. Qu, *Energ Environ Sci*, 2018, **11**, 1730-1735.
8. X. M. Liu, H. Y. Gao, J. E. Ward, X. R. Liu, B. Yin, T. D. Fu, J. H. Chen, D. R. Lovley and J. Yao, *Nature*, 2020, **578**, 550-554.
9. W. H. Xu, Y. X. Song, R. X. Xu and Z. K. Wang, *Advanced Materials Interfaces*, 2021, **8**.
10. F. Zhao, L. X. Wang, Y. Zhao, L. T. Qu and L. M. Dai, *Adv Mater*, 2017, **29**.
11. M. Jeong, J. Noh, M. Z. Islam, K. Kim, A. Sohn, W. Kim and C. Yu, *Adv Funct Mater*, 2021, **31**.
12. S. L. Kim, K. Choi, A. Tazebay and C. Yu, *Acs Nano*, 2014, **8**, 2377-2386.
13. S. L. Kim, J. H. Hsu and C. Yu, *Org Electron*, 2018, **54**, 231-236.
14. S. L. Kim, J. H. Hsu and C. Yu, *Nano Energy*, 2018, **48**, 582-589.
15. A. M. A. Mageeth, S. Park, M. Jeong, W. Kim and C. Yu, *Appl Energy*, 2020, **268**.
16. S. Lee, J. Eun and S. Jeon, *Nano Energy*, 2020, **68**.
17. T. Xu, X. T. Ding, Y. X. Huang, C. X. Shao, L. Song, X. Gao, Z. P. Zhang and L. T. Qu, *Energ Environ Sci*, 2019, **12**, 972-978.
18. F. Zhao, H. H. Cheng, Z. P. Zhang, L. Jiang and L. T. Qu, *Adv Mater*, 2015, **27**, 4351-4357.
19. F. Zhao, Y. Liang, H. H. Cheng, L. Jiang and L. T. Qu, *Energ Environ Sci*, 2016, **9**, 912-916.
20. Z. H. Lin, G. Cheng, S. Lee, K. C. Pradel and Z. L. Wang, *Adv Mater*, 2014, **26**, 4690+.
21. J. H. Nie, Z. M. Wang, Z. W. Ren, S. Y. Li, X. Y. Chen and Z. L. Wang, *Nat Commun*, 2019, **10**.
22. X. L. Wei, Z. H. Zhao, C. G. Zhang, W. Yuan, Z. Y. Wu, J. Wang and Z. L. Wang, *Acs Nano*, 2021, **15**, 13200-13208.
23. W. Xu, H. Zheng, Y. Liu, X. Zhou, C. Zhang, Y. Song, X. Deng, M. Leung, Z. Yang, R. X. Xu, Z. L. Wang, X. C. Zeng and Z. Wang, *Nature*, 2020, **578**, 392-396.
24. B. Fan, A. Bhattacharya and P. R. Bandaru, *Nat Commun*, 2018, **9**.
25. D. Z. Shen, M. Xiao, G. S. Zou, L. Liu, W. W. Duley and Y. N. Zhou, *Adv Mater*, 2018, **30**.
26. J. L. Xue, F. Zhao, C. G. Hu, Y. Zhao, H. X. Luo, L. M. Dai and L. T. Qu, *Adv Funct Mater*, 2016, **26**, 8784-8792.
27. Y. S. Qin, Y. S. Wang, X. Y. Sun, Y. J. Li, H. Xu, Y. S. Tan, Y. Li, T. Song and B. Q. Sun, *Angew Chem Int Edit*, 2020, **59**, 10619-10625.
28. H. Y. Wang, Y. L. Sun, T. C. He, Y. X. Huang, H. H. Cheng, C. Li, D. Xie, P. F. Yang, Y. F. Zhang and L. T. Qu, *Nat Nanotechnol*, 2021, **16**, 811+.
29. C. H. Yu, A. Murali, K. W. Choi and Y. Ryu, *Energ Environ Sci*, 2012, **5**, 9481-9486.
30. W. L. Liu, Z. Wang, G. Wang, G. L. Liu, J. Chen, X. J. Pu, Y. Xi, X. Wang, H. Y. Guo, C. G. Hu and Z. L. Wang, *Nat Commun*, 2019, **10**.
31. A. Sohn, J. H. Lee, H. J. Yoon, H. H. Lee and S. W. Kim, *Nano Energy*, 2020, **74**.
32. C. R. Liu, J. Sun, Y. Zhuang, J. Wei, J. Li, L. X. Dong, D. F. Yan, A. Hu, X. F. Zhou and Z. K. Wang, *Nanoscale*, 2018, **10**, 23164-23169.
33. W. H. Xu, X. F. Zhou, C. L. Hao, H. X. Zheng, Y. Liu, X. T. Yan, Z. B. Yang, M. Leung, X. C. Zeng, R. X. Xu and Z. K. Wang, *National Science Review*, 2019, **6**, 540-550.
34. Y. F. Zhang, A. Sohn, A. Chakraborty and C. Yu, *Nat Commun*, 2021, **12**.
35. L. Dong, L. Zhang, S. Lin, Z. X. Chen, Y. N. Wang, X. X. Zhao, T. Q. Wu, J. J. Zhang, W. Liu, H. B. Lu and K. P. Loh, *Nano Energy*, 2020, **70**.
36. S. Lin, L. Dong, J. J. Zhang and H. B. Lu, *Chem Mater*, 2016, **28**, 2138-2146.